https://doi.org/10.5194/egusphere-2026-360
Preprint. Discussion started: 13 February 2026

Convection-permitting projections of North American low-level jets and their mechanistic responses to climate change

Xiao Ma[1], Yanping Li[1], Fei Huo[1], Zhenhua Li[1]

[1]Western University, 1151 Richmond Street, London, Ontario N6A 3K7, Canada

Correspondence to: Yanping Li (yli4972@uwo.ca)

Abstract. This study investigates the response of North American Low-Level Jets (LLJs) to climate warming using a high-resolution (4 km) convection-permitting Weather Research and Forecasting (WRF) simulation driven by the Pseudo-Global Warming (PGW) approach. The simulation reveals that the response of LLJs is highly heterogeneous across seasons and regions. Among the various LLJ systems over North America, the most robust and dynamically distinct responses to climate warming are identified in the Great Plains southerly LLJ and the California coastal northerly LLJ. For the Great Plains southerly LLJ, the research identifies a robust intensification in spring but a muted response in summer. Mechanism analysis indicates that the spring strengthening is driven by a steepened zonal thermal gradient and enhanced nocturnal stability, which amplifies the inertial oscillation. In contrast, increased nocturnal instability in summer suppresses this decoupling mechanism, preventing significant strengthening. Regarding the California coastal northerly LLJ, the simulation projects a weakening trend in summer. This is attributed to a reconfiguration of the land-sea thermal contrast, where enhanced local sea-breeze circulations disrupt the coastal baroclinicity that sustains the jet. These results highlight the necessity of convection-permitting scales in capturing the fine-scale thermodynamic and dynamic adjustments governing future LLJ evolution. The projected seasonal shifts in jet intensity and vertical structure have important implications for other interdisciplinary fields.

1. Introduction

Low-level jets (LLJs) are narrow belts of strong winds embedded in the lower troposphere, typically characterized by a pronounced wind speed maximum within the lowest few kilometres of the atmosphere (Bonner, 1968; Rife et al., 2010). Despite their relatively shallow vertical extent, LLJs can span hundreds of kilometres horizontally and persist for hours. They often exhibit distinct diurnal and seasonal oscillations, which are tightly coupled with boundary layer processes and large-scale circulation patterns (Blackadar, 1957; Stensrud, 1996).

By efficiently transporting heat, moisture, and momentum, LLJs play a fundamental role in shaping regional weather and climate. In many continental and coastal regions, they serve as primary conduits for low-level moisture transport, significantly modulating precipitation distributions and providing favourable dynamic environments for convective initiation and extreme precipitation events (Walters and Winkler, 2001; Hodges and Pu, 2019; Tang et al., 2017). This climatological significance is particularly pronounced in regions such as the North American Great Plains and the eastern Pacific coast, where LLJs act as a critical link between synoptic-scale pressure systems and mesoscale weather processes. For instance, Weaver et al. (2012) found that the tornado activity in the southern United States is highly correlated with the intensity and location of the Great Plains LLJ. Beyond their impacts on weather and hydroclimate processes, LLJs hold substantial importance for various

https://doi.org/10.5194/egusphere-2026-360
Preprint. Discussion started: 13 February 2026

environmental and societal sectors. The strong vertical wind shear associated with LLJs affects wind energy generation efficiency and turbine structural loads (Banta et al., 2008). Furthermore, these systems modulate the transport and dispersion of atmospheric pollutants and influence aviation safety and urban climates by altering near-surface thermodynamic and dynamic conditions (Hu et al., 2013; Gadde and Stevens, 2021).

Given that the formation and maintenance of LLJs depend heavily on thermal gradients, boundary layer stability, and large-scale circulation structures (Blackadar, 1957; Holton, 1967; Uccellini et al., 1987), this system is expected to exhibit significant responses to anthropogenic climate warming. Consequently, in recent years, numerous researchers have utilized numerical products to investigate the response of LLJs to future climate change. Semedo et al. (2016) used the CMIP5 global climate model (GCM) to analyze worldwide Coastal Low-Level Jets (CLLJs) under the RCP8.5 scenario. Their results reveal that there is no consistent global trend in jet intensity or frequency, thereby future changes are region-dependent and governed by background circulation and local land-sea thermal structures. Tang et al. (2017) utilized the NARCCAP multi-model dynamic downscaling ensemble (~50 km) to investigate Great Plains LLJs (GPLLJs) in future scenarios. They found a significant future increase in nocturnal GPLLJ frequency, and this growth is concentrated over the southern plains in spring and moving to the central plains in summer, while changes during the daytime and cold season remain weak. Moreover, using an ensemble of 46 CMIP5 and CMIP6 models, Zhou et al. (2021) examined the co-variability of the GPLLJ, North Atlantic Subtropical High (NASH). It was concluded that the GPLLJ significantly strengthens and extends northward in spring and autumn, but with limited changes in summer, which is related to the structural adjustments of the NASH, not only the westward expansion of it.

Regional Climate Models (RCMs) have also been widely utilized in recent studies. Torres-Alavez et al. (2021) analyzed future changes in various global LLJ systems based on CORDEX-CORE regional climate simulations (~25 km resolution). Results indicate that under warming scenarios, most LLJs exhibit a general trend of strengthening and spatial migration. However, the magnitude of changes varies across different regions and LLJ types, displaying strong spatial heterogeneity. Similarly, Juliano et al. (2025) employed WRF regional climate simulations (~25 km) to examine future changes in the California Coastal Low-Level Jet (CLLJ) using Self-Organizing Maps (SOM). It is found that the frequency of LLJ increases in Northern California but decreases in Southern California. Furthermore, they noted that changes in LLJ intensity are highly sensitive to the driving GCMs. Based on the conclusions of the above studies, it is evident that RCMs capture greater local spatial heterogeneity in predicting future LLJ changes, making them more informative than GCMs.

However, most conventional numerical models still rely on convective parameterization schemes to represent convective processes, thereby introducing significant uncertainties in simulating low-level dynamic structures and associated weather systems. The application of convection-permitting models (CPMs) with grid spacing of less than 5 km can largely overcome this limitation, as these models are capable of explicitly resolving deep convection and other critical meso- and small-scale processes (Liu et al., 2017; Li et al., 2019; Ma et al., 2022). Compared to coarse-resolution simulations and reanalysis data, CPMs exhibit distinct advantages in characterizing surface features over complex terrain and their interactions with LLJs (Zhang et al., 2022). Ma et al. (2024) provided the first systematic characterization of typical North American LLJs by 4km WRF simulations, including the Great Plains S-LLJ, California Coastal N-LLJ, and Quebec Winter N-LLJ. This study highlighted the capability of

https://doi.org/10.5194/egusphere-2026-360
Preprint. Discussion started: 13 February 2026

CPMs to capture mesoscale wind systems in complex terrain and coastal areas. Mu et al. (2025) further extended the application of 4 km WRF simulations to analyze the Northerly LLJ east of the Andes, revealing its critical role in modulating Mesoscale Convective Systems (MCSs). They found that stronger LLJs facilitate the organization of larger, longer-duration, and heavier-precipitation convective systems at the jet exit. Together, these findings underscore the superiority of CPMs over coarse-resolution models in resolving fine-scale LLJ structures and their associated impacts.

Despite the great potential of CPMs in characterizing the fine structure of LLJs, research using these high-resolution models to explore the LLJ's response to future climate change is still limited. Thus, to expand our in-depth understanding of the local variability and physical mechanisms of the LLJ under future climate conditions, this study aims to employ the 4 km convection-permitting WRF simulation to project the future evolution of North American LLJ systems. Section 2 describes the model configuration and the criteria used for LLJ identification. Section 3 examines the seasonal climatology of LLJs and evaluates their responses to future climate. Section 4 investigates the specific changes and underlying dynamic mechanisms of several typical regional LLJ systems. Finally, Section 5 provides a discussion and summary of the key findings.

2 Model configuration and methods

2.1 Model setup

The simulations were performed using WRF 3.4.1 at a 4-km convection-permitting resolution (Liu et al., 2017). The domain covers the continental United States (CONUS), southern Canada (up to ~52°N), and northern Mexico (shown in Figure 1). The simulation spans the period from October 2000 to September 2013, providing model outputs of 3D variables at 3-hour intervals and 2D variables at 1-hour intervals. Initial and lateral boundary conditions were provided by the ERA-Interim reanalysis dataset. Notably, the vertical grid is configured with 5 layers within the lowest 500 m and 9 layers within the lowest 1 km above ground level (AGL). This fine vertical resolution implies that the WRF model is better equipped to capture LLJs within the boundary layer compared to coarser-resolution models.

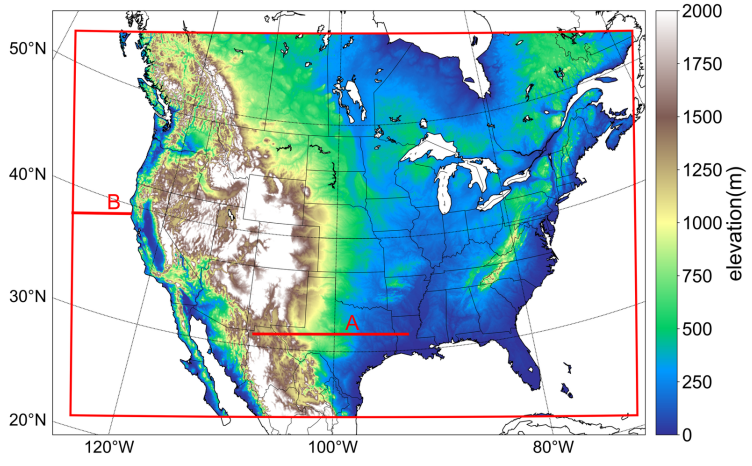

https://doi.org/10.5194/egusphere-2026-360
Preprint. Discussion started: 13 February 2026

Figure 1. Model domain of the convection-permitting simulation. Colours indicate terrain elevation. The red lines mark the cross-sections of the analyzed LLJs in Section 4.

Given the high horizontal resolution of 4 km, cumulus parameterization was not adopted in this study to allow for explicit convection. The physical parameterization schemes selected for this study include: the Rapid Radiative Transfer Model for GCMs (RRTMG) for both longwave and shortwave radiation processes (Iacono et al., 2008); the Yonsei University (YSU) scheme for planetary boundary layer (PBL) turbulence (Hong et al., 2006); and the modified Noah-MP land surface model for surface processes (Niu et al., 2011).

Based on the model configuration described above, two sets of numerical experiments were conducted: a Control Run (CTRL) representing current climate conditions, and a Pseudo-Global Warming (PGW) Run representing future climate change. In the PGW experiment, climate change perturbations derived from the CMIP5 multi-model ensemble mean were superimposed onto the ERA-Interim boundary conditions to drive the regional climate simulation. This perturbation signal was calculated from the ensemble mean change of 19 Global Climate Models (GCMs) (Liu et al., 2017). The future scenario follows the Representative Concentration Pathway 8.5 (RCP8.5), corresponding to an atmospheric CO2 concentration of approximately 1350 ppm and a radiative forcing of ~8.5 W m^{-2} by the end of the 21st century (Taylor et al., 2012). The ensemble mean climate difference was obtained by comparing the historical period (1976–2005) with the future period (2071–2100). Thus, the perturbation represents a climate change signal over a timescale of approximately 95 years, expressed as follows:

$$\Delta CMIP5_{RCP8.5} = CMIP5_{2071-2100} - CMIP5_{1976-2005}\,, \quad (1)$$

And then, add this perturbation with ERA-Interim data to get the initial condition of PGW simulation:

$$WRF_{input} = ERA_{Interim} + \Delta CMIP5_{RCP8.5}\,, \quad (2)$$

Although a 13-year duration is shorter than typical climatological studies, it represents a strategic compromise for high-resolution simulations to ensure computational efficiency. Crucially, the PGW approach obviates the need for extended simulations; it allows for centennial-scale projections to be derived from just 13 years of data through equivalent climate perturbations.

2.2 Methods

In this study, the classical criteria proposed by Bonner (1968) are applied to identify LLJs from the vertical wind profiles at each grid derived from the model output. An LLJ is defined when all of the following conditions are satisfied: (1) the height of the jet core is located within 3 km above ground level; (2) the maximum wind speed at the jet core is ≥ 12 m s^{-1}; (3) the wind speed decreases by at least 6 m s^{-1} both upward from the level of maximum wind speed to the next wind-speed minimum (or to 3 km AGL, whichever is lower) and downward from the jet core toward the surface. In addition, LLJs are further categorized based on the wind direction at the jet core (Walter et al., 2008; Doubler et al., 2015). LLJs with core wind directions between 113° and 247° are classified as southerly LLJs (S-LLJs), whereas those with core wind directions between 293° and 67° are classified as northerly LLJs (N-LLJs).

https://doi.org/10.5194/egusphere-2026-360
Preprint. Discussion started: 13 February 2026

3. Seasonal Variations and Future Climate Responses of LLJs

3.1 Southerly LLJs

3.1.1 Occurrence Frequency

Figure 2 summarizes the seasonal occurrence frequency of southerly low-level jets (S-LLJs) in the CTRL simulation (Fig. 2a–d) and their projected changes under the PGW scenario (Fig. 2e–h). In the current climate, S-LLJs exhibit a pronounced seasonal cycle, with the highest occurrence in spring and summer and markedly weaker activity during the cold season. The spring S-LLJ forms a spatially extensive high-frequency corridor (>15–20%) extending from northeastern Mexico through the Great Plains into the Canadian Prairies, while summer activity becomes more confined, with a northward-shifted and zonally narrower core centered over the central Great Plains. In contrast, S-LLJ occurrence decreases rapidly in autumn and reaches its annual minimum in winter, when significant activity is largely restricted to southern Texas and northeastern Mexico. These seasonal characteristics are broadly consistent with previous analyses of S-LLJ climatology (Ma et al., 2024).

Under the PGW scenario, S-LLJ occurrence generally increases across North America, although the magnitude and spatial extent of the response exhibit strong seasonal dependence. The most pronounced and spatially coherent enhancement occurs in spring (Fig. 2e), with widespread increases of 1–3% extending from northeastern Mexico through the central Great Plains to South Dakota. The strongest signals are concentrated over the present-day S-LLJ core between Texas and Kansas, where local increases exceed 3% and statistical significance is widespread. Weaker but coherent positive anomalies (~1%) are also evident over the southern Canadian Prairies, northern Ontario, and western Quebec, while an additional enhancement of approximately 3% appears along the downstream side of the Appalachian Mountains, associated with the coastal S-LLJ.

In summer (Fig. 2f), the area of increased S-LLJ occurrence contracts substantially relative to spring. Significant positive changes exceeding 2% are largely confined to the central Great Plains (e.g., Kansas and Oklahoma) and the southeastern Texas coast. In contrast, northeastern Mexico exhibits a clear reduction in S-LLJ frequency, with local decreases approaching −3%, indicating a potential eastward displacement of the active summer S-LLJ region under future climate conditions. Over Canada, only a small and spatially limited increase of approximately 1% is found in southern Saskatchewan. Notably, the coastal S-LLJ near the Appalachian Mountains shows a stronger summer response than in spring, with frequency increases exceeding 3%.

Autumn represents the second-strongest season of positive S-LLJ frequency changes (Fig. 2g). Although weaker than the spring signal, the enhancement remains spatially coherent and is concentrated over regions with high present-day S-LLJ activity. Core areas in Oklahoma, Kansas, and Missouri experience increases of approximately 1–2%, with weaker but still positive anomalies (~1%) extending northward into southern Nebraska and parts of South Dakota. By contrast, winter exhibits the weakest and most spatially restricted response among all seasons (Fig. 2h). Positive changes of 1–2% are confined primarily to a narrow corridor from southern Texas to Louisiana, accompanied by a slight negative trend (~−1%) over the northwestern Gulf of Mexico. Overall, the projected S-LLJ frequency response under PGW is characterized by a strong spring maximum, a muted midsummer signal, and limited wintertime changes.

https://doi.org/10.5194/egusphere-2026-360
Preprint. Discussion started: 13 February 2026

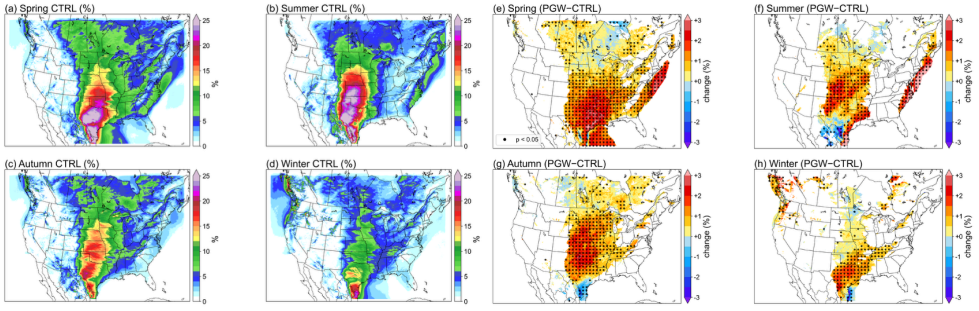

Figure 2. Seasonal occurrence frequency of S-LLJs in the CTRL simulation (a-d) and their projected changes under the PGW simulation (e-h). Black dots mark areas where differences are statistically significant at the 95% confidence level, and the regions which frequency is lower than 5% are masked in fig. 2e to 2h.

3.1.2 Intensity

To characterize the strength of southerly low-level jets (S-LLJs), we examine the mean maximum wind speed at the jet core for identified events, with regions of low occurrence (<5%) masked. Figure 3 shows the seasonal distribution of S-LLJ core wind speeds in the CTRL simulation (Fig. 3a–d) and their projected changes under the PGW scenario (Fig. 3e–h).

In the current climate, S-LLJ core wind speeds exhibit clear seasonal contrasts. Spring features the strongest and most spatially extensive intensities, forming a continuous high-speed corridor from northern Texas across the Great Plains to eastern Canada, with typical core speeds of 18–20 m s^{-1} and local maxima exceeding 22 m s^{-1}. In summer, the high-wind region contracts markedly, with elevated core speeds largely confined to the central Great Plains, while autumn represents a transitional state characterized by a southwest–northeast contrast, with weaker winds over the southern Great Plains and stronger cores extending into eastern Canada. Despite reduced occurrence, winter S-LLJs maintain relatively high core intensities along a narrow north–south corridor, with wind speeds commonly exceeding 18 m s^{-1}.

Projected changes in S-LLJ core wind speed under PGW display pronounced seasonality. Spring shows the most spatially coherent intensification (Fig. 3e), with widespread positive anomalies extending from northern Texas through the central Great Plains into Alberta, generally exceeding 0.3 m s^{-1} and locally surpassing 0.5 m s^{-1}. In contrast, summer responses are weak and spatially limited (Fig. 3f), with most of the Great Plains exhibiting near-zero changes and only localized strengthening (~0.4 m s^{-1}) along the Texas coast and in parts of the central Canadian Prairies. The coastal S-LLJ east of the Appalachian Mountains also shows a clear and statistically significant summer intensification.

Autumn exhibits a distinct meridional contrast in the intensity response (Fig. 3g), with robust strengthening over the northern Great Plains and south-central Canada, where anomalies commonly exceed 0.5 m s^{-1}, while changes over the southern Great Plains remain small or slightly negative. Winter displays the weakest overall response (Fig. 3h), with modest positive anomalies confined mainly to Texas and Oklahoma and slight reductions over much of the central and northern Great Plains.

https://doi.org/10.5194/egusphere-2026-360
Preprint. Discussion started: 13 February 2026

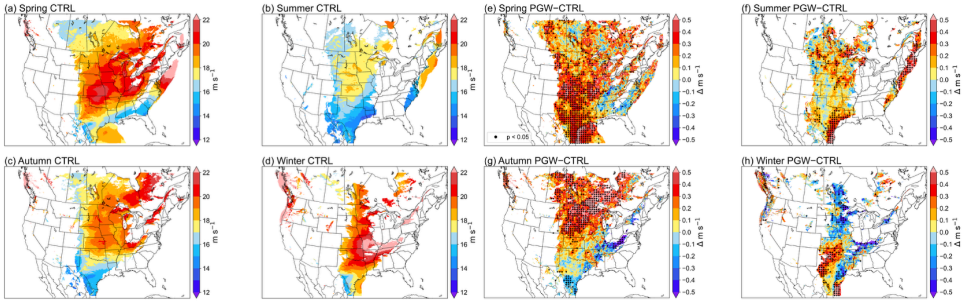

Figure 3. Seasonal mean wind speed of the S-LLJs core in the CTRL simulation (a-d) and their projected changes under the PGW simulation (e-h). Black dots mark areas where differences are statistically significant at the 95% confidence level, and the regions which frequency is lower than 5% are masked in all subplots

3.1.3 Jet Height

Figure 4 presents the seasonal climatology of S-LLJ core height in the CTRL simulation and its projected changes under the PGW scenario, with regions of low occurrence (<5%) masked. In the current climate, S-LLJ cores are generally confined to the lower boundary layer along the Great Plains axis, with typical heights clustered around 500–600 m throughout most of the year. Superimposed on this relatively shallow background, the core height exhibits systematic seasonal and meridional variations. In spring and autumn, higher core elevations occur over the southern Great Plains, where heights locally exceed 750 m, while northern regions remain substantially lower. Summer is characterized by the lowest and most spatially uniform core heights over the Great Plains, whereas winter features the highest core elevations over the reduced active region, particularly from southern Texas to the lower Mississippi River valley.

In the future scenario, S-LLJ core height shows a clear and seasonally dependent response. In spring (Fig. 4e), a coherent band of positive anomalies develops along the Great Plains, extending from northern Texas into southern Canada, with height increases typically of 20–40 m and locally exceeding 60–80 m. In summer (Fig. 4f), height increases become more spatially concentrated, with pronounced rises of 60–80 m—and locally above 100 m—over Texas, indicating an upward shift of S-LLJ cores in the southern United States. Autumn exhibits a north–south contrast (Fig. 4g), with moderate height increases (20–40 m) extending from Kansas into the central Canadian Prairies and minimal changes over the southern Great Plains. Winter represents the sole season dominated by negative anomalies (Fig. 4h), with a continuous band of core height reductions from Texas to the lower Mississippi River valley reaching −40 to −80 m and locally exceeding −100 m. Overall, the projected height response indicates a systematic rise of S-LLJ cores during the warm season and a pronounced lowering in winter, pointing to a seasonally reorganized vertical structure of the lower troposphere under future climate conditions.

https://doi.org/10.5194/egusphere-2026-360
Preprint. Discussion started: 13 February 2026

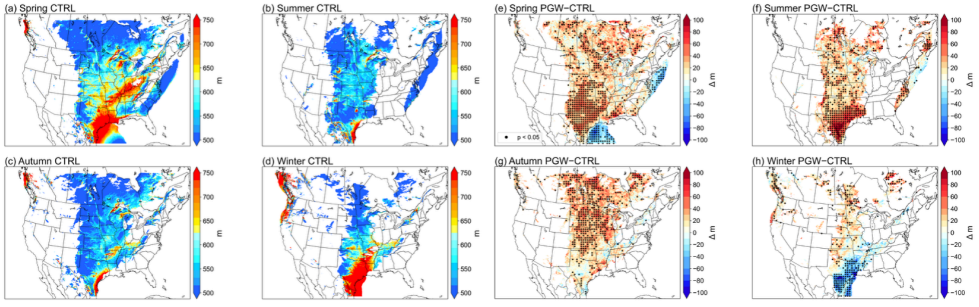

Figure 4. Seasonal mean core height of the S-LLJs in the CTRL simulation (a-d) and their projected changes under the PGW simulation (e-h). Black dots mark areas where differences are statistically significant at the 95% confidence level, and the regions which frequency is lower than 5% are masked in all subplots

3.2 Northerly LLJs

3.2.1 Occurrence Frequency

Similarly, the seasonal occurrence frequency of N-LLJs in the current climate and the corresponding changes in the PGW are also depicted in Figure 5. In the current climate, N-LLJs exhibit pronounced regional and seasonal contrasts. During spring, N-LLJ activity is limited, with two primary centers along the California coast and over the Quebec Plateau. The California coastal jet begins to establish as a warm-season feature, forming a narrow band with frequencies exceeding 10%, while most of the continental interior shows weak activity. In summer, the California coastal N-LLJ becomes the dominant system across the domain, with core frequencies exceeding 25% and extending from southern Oregon to central California and offshore. As the cold season approaches, N-LLJ activity expands inland. Autumn is characterized by the reemergence of orographic jets from the eastern slopes of the Rocky Mountains into the Canadian Prairies, accompanied by increasing activity over eastern Canada, while winter features the strongest cold-season N-LLJs over the continental interior and the Quebec–Labrador Plateau, where frequencies commonly exceed 20–25%.

The future response of N-LLJ occurrence differs markedly among regional systems. Along the California coast, N-LLJ frequency increases in spring, summer, and autumn, with positive anomalies generally exceeding 2%. In summer, however, a narrow band of negative anomalies (approaching −3%) appears immediately along the coastline and transitions offshore into significant positive anomalies, indicating a modest offshore displacement of the coastal N-LLJ in a warmer climate. Because N-LLJ activity over the continental interior is minimal during summer in the CTRL simulation, no coherent summer response is found in these regions.

By contrast, the cold-season N-LLJ over the Quebec–Labrador Plateau shows a systematic reduction in occurrence outside of summer. The largest decreases occur in winter, with anomalies exceeding −3%, suggesting a weakened persistence of this terrain-forced jet under future conditions. The orographic N-LLJ system east of the Rocky Mountains exhibits a more nuanced response: changes remain weak and spatially scattered in spring. At the same time, autumn shows a narrow belt of modest negative anomalies (~−1%) extending from Alberta to Wyoming. In winter, a coherent band of positive anomalies develops across the northern Great Plains and southern Canadian Prairies, with increases of 1–2%.

https://doi.org/10.5194/egusphere-2026-360
Preprint. Discussion started: 13 February 2026

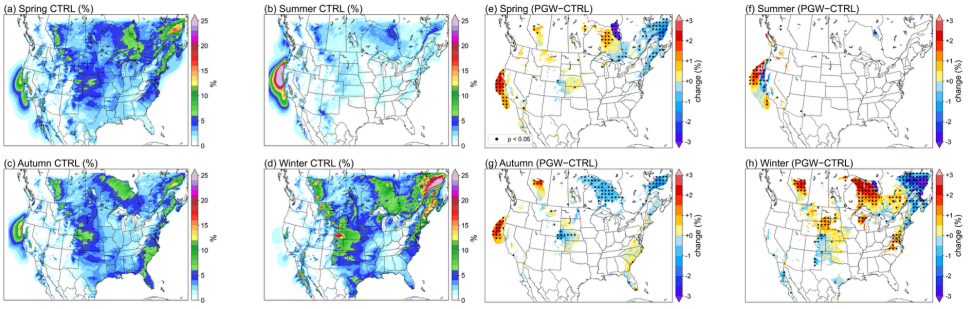

Figure 5. Seasonal occurrence frequency of N-LLJs in the CTRL simulation (a–d) and their projected changes under the PGW simulation (e–h). Black dots denote grid points with statistically significant differences at the 95% confidence level; areas with CTRL frequency <5% are masked in panels (e–h).

3.2.2 Intensity

The core mean wind speeds of the N-LLJs are offered in Figures 6a-d, and their structures also exhibit distinct regional features. First, in the current climate, N-LLJ intensity exhibits pronounced system-dependent characteristics. The California coastal N-LLJ is the most persistent high-intensity system throughout the year, with core wind speeds commonly reaching 20–22 m s^{-1} from spring through autumn and peaking in summer, forming a narrow but intense coastal jet. By contrast, the Quebec N-LLJ displays a clear cold-season dominance, with winter core wind speeds also reaching 20–22 m s^{-1}, while its structure weakens substantially during the transitional seasons. The inland N-LLJ east of the Rocky Mountains forms a distinct cold-season high-speed corridor from southern Alberta to Colorado, with winter core wind speeds often near 20 m s^{-1} and reduced intensities (~18 m s^{-1}) during spring and autumn.

The projected response of N-LLJ core wind speed under PGW varies strongly among regional systems. Along the California coast, the N-LLJ intensifies in spring and autumn, with positive anomalies of 0.3–0.5 m s^{-1} concentrated along the northern-to-central coast and locally exceeding 0.5 m s^{-1}. In contrast, summer exhibits a marked weakening, with negative anomalies approaching −0.4 m s^{-1} along the south-central coast, indicating an opposite warm-season response relative to the transitional seasons. Over northeastern Canada, the Quebec N-LLJ shows the most spatially extensive and robust intensification in winter, with positive anomalies of approximately 0.5 m s^{-1} covering much of the region. Changes in the inland N-LLJ east of the Rocky Mountains remain comparatively weak and spatially fragmented across seasons, lacking a coherent large-scale signal. Overall, the intensity response of N-LLJs to future warming is dominated by system-specific dynamics, resulting in strong regional contrasts and pronounced seasonal asymmetry.

https://doi.org/10.5194/egusphere-2026-360
Preprint. Discussion started: 13 February 2026

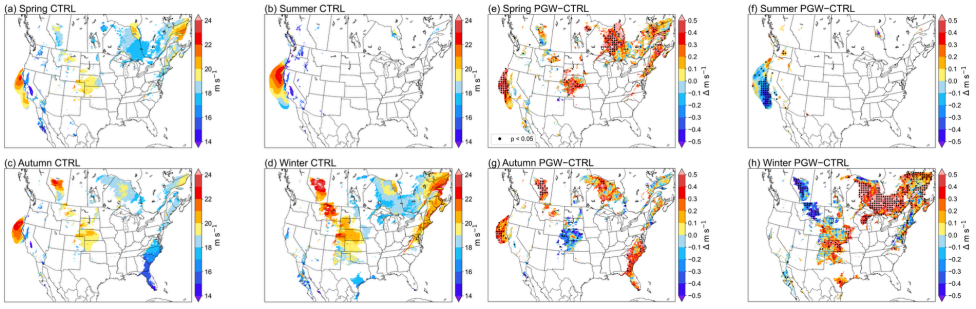

Figure 6. Seasonal mean wind speed of the N-LLJs core in the CTRL simulation (a-d) and their projected changes under the PGW simulation (e-h). Black dots mark areas where differences are statistically significant at the 95% confidence level, and the regions which frequency is lower than 5% are masked in all subplots

3.2.3 Jet height

The vertical structure of N-LLJs in the CTRL simulation exhibits pronounced regional contrasts, while the degree of seasonal variability differs substantially among individual systems. Along the California coast, N-LLJ core heights show a distinct and persistent summer feature, with a pronounced decrease from the open ocean toward the nearshore region, as evident in Figure 7b. Core heights over the open ocean commonly approach 600 m but rapidly decline to approximately 350 m near the coast, forming a sharp land–sea gradient that is largely absent in other seasons. By contrast, the Quebec N-LLJs are most prominent during spring, autumn, and winter, and their core heights display strong seasonal modulation. During the transitional seasons, core heights are generally elevated, typically approaching 600 m, whereas in winter they decrease markedly to around 400 m (Fig. 7d). Inland N-LLJs downstream of the Rocky Mountains are comparatively limited in spatial extent and exhibit little seasonal dependence, with core heights remaining near 600 m throughout the year. Taken together, the CTRL climatology highlights clear regional contrasts in N-LLJ core height, with a pronounced nearshore-decreasing structure along the California coast in summer and strong seasonal variability over eastern Canada.

Future changes in N-LLJ core height are generally modest and spatially confined, with coherent responses emerging only in a few key regions. Over the California coast, a clear height response appears exclusively in summer, when the N-LLJ core shifts downward relative to the CTRL climatology (see Fig. 7f). Reductions of approximately 40 m occur near the coast, with even larger decreases offshore, producing negative anomalies that intensify seaward. Given that the present-day core height already decreases from offshore toward the coast, this pattern points to a weakened cross-shore height gradient under future warming. In eastern Canada, the Quebec N-LLJ exhibits the most pronounced height response in winter, with widespread positive anomalies and core heights increasing by more than 100 m, as illustrated in Figure 7h. Height changes during spring and autumn remain comparatively weak in this region. Meanwhile, inland N-LLJs east of the Rocky Mountains show no coherent height response across seasons, with variations remaining weak and spatially scattered in Figures 7e–h.

https://doi.org/10.5194/egusphere-2026-360
Preprint. Discussion started: 13 February 2026

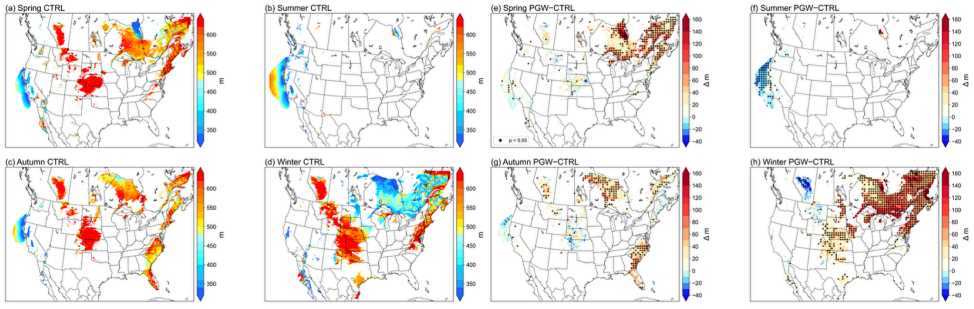

Figure 7. Seasonal mean core height of the N-LLJs in the CTRL simulation (a-d) and their projected changes under the PGW simulation (e-h). Black dots mark areas where differences are statistically significant at the 95% confidence level, and the regions which frequency is lower than 5% are masked in all subplots.

3.3 Monthly Characteristics of Representative LLJ Systems

The preceding sections have characterized the seasonal behaviour of different LLJ systems and their responses to future warming. However, seasonal-mean diagnostics can obscure important intra-annual variations, particularly when changes are concentrated within specific months. To better resolve the temporal evolution of LLJ activity and to illustrate contrasts between distinct systems, the following analysis focuses on two representative cases: the Great Plains S-LLJ and the California coastal N-LLJ. Owing to their contrasting spatial structures and forcing mechanisms, these systems provide an instructive framework for examining monthly-scale variability.

For the Great Plains S-LLJ, the analysis is restricted to its core summer activity region, defined using grid points where the summer occurrence frequency exceeds 15% within the selected domain (Fig. 8a). Monthly S-LLJ occurrence frequency and core wind speed are then computed based on these filtered grid points, with error bars representing the spatial dispersion within the region. The resulting monthly evolution of S-LLJ frequency and intensity under the CTRL and PGW simulations is summarized in Figures 8b and 8c. The monthly evolution of S-LLJ occurrence frequency reveals a pronounced seasonal progression. In the CTRL simulation, S-LLJ frequency increases steadily from winter, reaches its annual maximum during late spring to early summer (May–June; about 22–24%), and subsequently weakens through midsummer and autumn before attaining a minimum in January (Fig. 8b). Under future warming, the overall phase of the annual cycle remains largely unchanged, but S-LLJ occurrence is systematically enhanced during most months. The strongest increases are concentrated in late spring and early summer, when peak-month frequencies rise by roughly 2–3 percentage points relative to CTRL. By contrast, during midsummer (July–August), the PGW–CTRL differences are markedly smaller, indicating a muted response during the summer.

The error-bar structure further highlights this contrast. Spatial variability among grid points is lowest in midsummer, whereas substantially larger dispersion is evident in May and June, suggesting that future changes in GP S-LLJ occurrence are both stronger and more spatially heterogeneous during the seasonal transition period. Taken together, these monthly results demonstrate that the largest increases in GP S-LLJ activity occur prior to the midsummer maximum, a feature that is not readily apparent from seasonal-mean diagnostics alone and helps explain the spring-dominated signal identified in Section 3.1.

https://doi.org/10.5194/egusphere-2026-360
Preprint. Discussion started: 13 February 2026

Meanwhile, Figure 8c shows that the monthly evolution of S-LLJ core wind speed provides a useful contrast to the occurrence frequency. The CTRL core wind speed increases from winter into spring, reaching ~19–20 m s^{-1} in mid-to-late spring, before weakening to a midsummer minimum of ~15–16 m s^{-1} and recovering in autumn. Under future warming, the annual phase of the wind-speed cycle remains largely unchanged, with modest intensification in most months. Increases are typically 0.2–0.5 m s^{-1} in spring and autumn but are much smaller in midsummer (~0.1 m s^{-1}). Compared with the pronounced monthly variations in occurrence frequency, the variability of core wind speed is limited, with standard deviations generally within 1–2 m s^{-1}, indicating relatively uniform intensity across the core region.

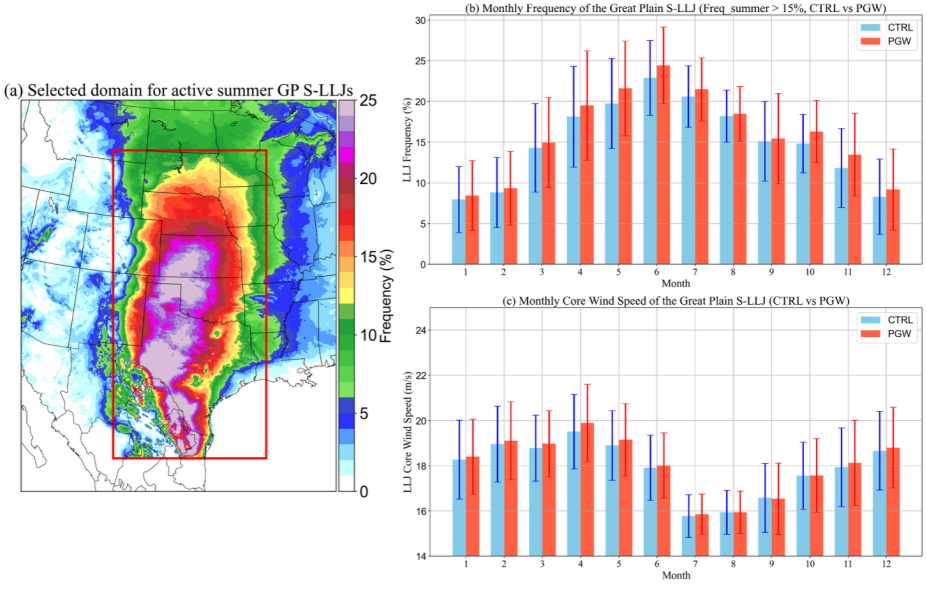

Figure 8. (a) Selected domain for the Great Plains S-LLJ analysis (red box). (b) Monthly occurrence frequency of the Great Plains S-LLJ under the CTRL and PGW scenarios. (c) Monthly mean core wind speed of the Great Plains S-LLJ under the CTRL and PGW scenarios. Error bars denote the spatial standard deviation within the core activity region.

As shown in Figure 9, the California coastal N-LLJ exhibits a substantially stronger annual variation on the monthly scale than the Great Plains S-LLJ. In the CTRL simulation, the occurrence frequency of the California coastal N-LLJ decreases to nearly zero during winter, followed by a rapid increase from early spring, with a pronounced rise during March–June. In contrast, the Great Plains S-LLJ maintains a non-negligible occurrence frequency throughout winter, resulting in a much smoother annual cycle. This contrast is consistent with the seasonal characteristics identified in Section 3.2, confirming the stronger warm-season dominance of the California coastal N-LLJ.

Under the PGW scenario, the phase of the monthly cycle for the California coastal N-LLJ remains largely unchanged relative to CTRL, but its annual amplitude is noticeably modified. Increases in occurrence frequency are primarily concentrated in spring to early summer, with the most pronounced enhancement occurring during March–June. In contrast, during midsummer (July–August), although the California coastal N-LLJ still represents

https://doi.org/10.5194/egusphere-2026-360
Preprint. Discussion started: 13 February 2026

359 the annual peak in occurrence frequency, its frequency is clearly reduced relative to CTRL. This behaviour
360 indicates that future warming does not induce a systematic phase shift in the monthly cycle but instead leads to a
361 weakening of the peak-season amplitude.

362 Compared with occurrence frequency, the monthly variability of core wind speed for the California coastal N-
363 LLJ is considerably weaker. In both the CTRL and PGW simulations, core wind speed exhibits only modest
364 annual variation, indicating a relatively stable intensity throughout the year. Nevertheless, a subtle but coherent
365 signal can still be identified; the PGW core wind speeds tend to be slightly enhanced during late spring to early
366 summer (April–May), while a more evident weakening emerges during July–August. Differences in other months
367 remain small. These results suggest that, for the California coastal N-LLJ, future changes are dominated by a
368 redistribution of occurrence on the monthly scale, whereas modifications to individual event intensity are
369 secondary and largely confined to the midsummer period.

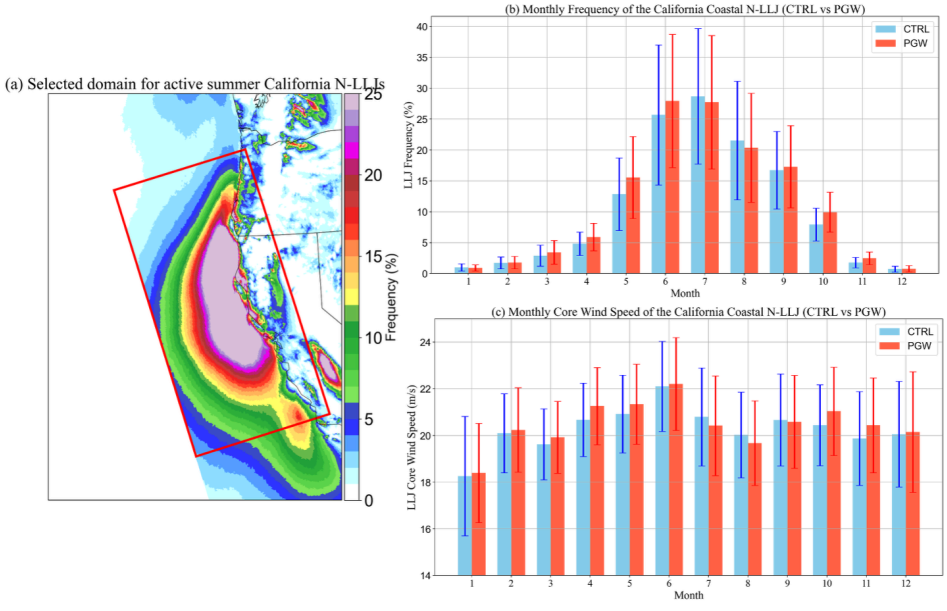

370

371 **Figure 9. (a) Selected domain for the California coastal N-LLJ analysis (red box). (b) Monthly occurrence frequency**
372 **of the California coastal N-LLJ under the CTRL and PGW scenarios. (c) Monthly mean core wind speed of the**
373 **California coastal N-LLJ under the CTRL and PGW scenarios. Error bars denote the spatial standard deviation**
374 **within the core activity region.**

375 **4. Mechanisms analysis underlying the PGW response of LLJs**

376 The results in Section 3 indicate that different types of LLJs exhibit significant differences in their response to
377 warming under the PGW scenario. Notably, over the Great Plains, the S-LLJ shows a marked enhancement in
378 both occurrence frequency and jet core wind speeds during the spring, whereas the magnitude of these changes is
379 significantly weaker in the summer. In contrast, the California coastal N-LLJ displays a response pattern that
380 differs from the inland jets. Since statistical results alone are insufficient to explain these discrepancies, it is
381 necessary to investigate further the underlying causes from the perspective of dynamic structures.

https://doi.org/10.5194/egusphere-2026-360
Preprint. Discussion started: 13 February 2026

In our previous work (Ma et al., 2024), we systematically analyzed the formation mechanisms of major North American LLJs under the current climate. We highlighted that the nocturnal enhancement of the Great Plains S-LLJ is dominated by the inertial oscillation theory, while the California coastal N-LLJ is primarily driven by baroclinicity and sea-land thermal contrast. Building on this theoretical framework, this study further investigates whether these existing dynamic processes are altered under a warming climate, and how such alterations lead to the differential responses of LLJs across different seasons and types.

To this end, this study selects two representative jet core locations (refer to Points A and B in Fig. 1) to conduct a targeted diagnosis of the low-level wind structure under the CTRL and PGW scenarios. Point A is located in Texas, a typical active region for the Great Plains S-LLJ. During the PGW scenario, this region exhibits the most significant LLJ enhancement during spring, characterized by a simultaneous increase in both occurrence frequency and core wind speed, with increments of 3 percentage points and 0.3 m s^{-1}, respectively. In contrast, only slight changes are observed in summer. And the Point B is situated along the California coast, serving as a typical core area for the summertime California coastal N-LLJ. According to the preceding statistical analysis, the responses at Point B during spring and summer exhibit distinct positive/negative contrasts. Selecting Point B helps to assess whether the background geostrophic wind structure and the associated low-level dynamic constraints of the coastal LLJ undergo systematic changes under a warming climate.

4.1 Great Plains S-LLJ

In a mechanism analysis, it should select representative scenarios with the most significant differences in climate response to highlight key physical processes. For the Great Plains S-LLJ, Fig. 8 in subsection 3.3 indicates distinct differences in its response to warming between spring and summer. Specifically, May and August represent the two states with the most typical and divergent signals for these respective seasons.

Meanwhile, according to the inertial oscillation theory of Blackadar (1957), the actual low-level wind can be divided into the sum of geostrophic and ageostrophic winds:

$$\vec{\boldsymbol{V}} = \vec{\boldsymbol{V}}_{\boldsymbol{g}} + \vec{\boldsymbol{V}}_{\boldsymbol{a}}\,, \tag{3}$$

In the evening, after the boundary layer stabilizes and near-surface friction weakens significantly, the evolution of the ageostrophic wind is primarily controlled by the Coriolis force, resulting in an approximately circular periodic rotation trajectory within a diurnal cycle:

$$\frac{d\vec{\boldsymbol{V}}_{\boldsymbol{a}}}{dt} + \vec{\boldsymbol{f}} \times \vec{\boldsymbol{V}}_{\boldsymbol{a}} \approx \boldsymbol{0}\,, \tag{4}$$

This theory provides a classical dynamical framework for explaining the nocturnal formation of LLJs: when the ageostrophic wind rotates from a direction approximately opposite to the geostrophic wind to align with it, their superposition causes the actual wind to transition from a subgeostrophic to a supergeostrophic state, thereby generating significant wind speed enhancement at low levels. Essentially, this process originates from the unbalanced adjustment of the wind field triggered by the decoupling of the boundary layer from surface friction effects.

https://doi.org/10.5194/egusphere-2026-360
Preprint. Discussion started: 13 February 2026

Figure 10 shows the mean geostrophic wind vectors and the mean diurnal hodographs of the actual wind at the jet core height in May and August. The black and gray arrows denote the mean geostrophic winds in the CTRL and PGW scenarios, while the blue and red curves represent the diurnal evolution of the actual winds, respectively. In May (Fig. 10a), the mean geostrophic wind over the Great Plains S-LLJ region is stronger in the PGW scenario, indicating a systematic enhancement of the background pressure gradient. The hodograph of the actual wind also expands outward during the evening to nighttime period (18–03 CST, corresponding to 00–09 UTC in figures), and its shape becomes closer to a circular pattern. This outward expansion reflects a larger rotation radius and stronger amplitude of the ageostrophic wind, suggesting that the inertial oscillation becomes more pronounced under future warming. As a result, the superposition between the ageostrophic and geostrophic components is enhanced at night, which favours stronger supergeostrophic acceleration and the intensification of the nocturnal LLJ.

In contrast, the hodograph trajectory of the actual wind in August (Fig. 10b) exhibits a structure that is generally more circular than that in May. This indicates that the inertial oscillation signal is more typical under summer background conditions. However, the mean geostrophic wind is slightly weaker for the PGW simulation, implying a reduced large-scale pressure gradient. Meanwhile, the radius of the hodograph is also obviously smaller than that in CTRL, suggesting a weakening of the ageostrophic wind amplitude and the inertial oscillation effect. The combined weakening of both the background geostrophic wind and the ageostrophic oscillation is consistent with the statistical results, which show only slight enhancement or even a weakening tendency of the Great Plains S-LLJ in summer.

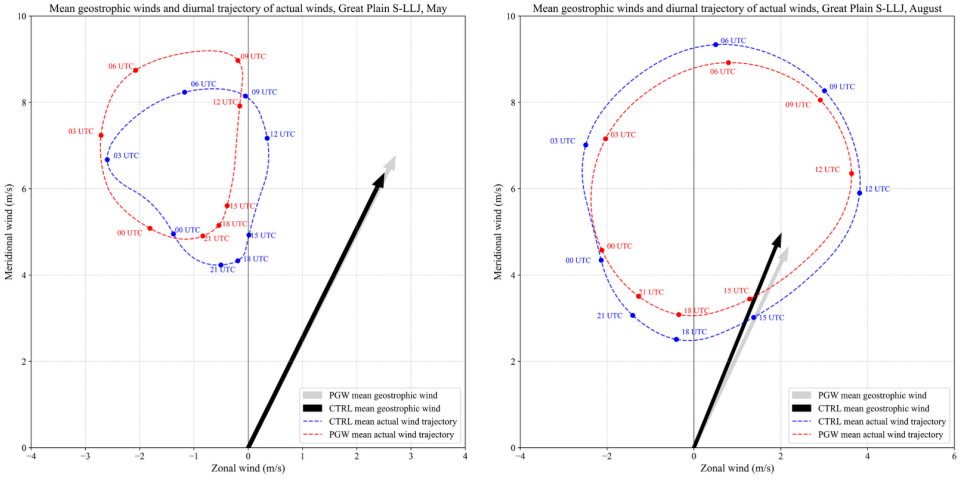

Figure 10. Mean geostrophic winds and the diurnal variation of actual winds at the core height of the S-LLJ over the Great Plains: (a) May, (b) August.

To further examine the thermal and stratification backgrounds associated with the different seasonal responses of LLJs to climate warming, Fig. 11 shows a meridional cross-section through Point A, including the mean wind speed and potential temperature in CTRL, as well as the PGW-induced changes in meridional wind, potential

https://doi.org/10.5194/egusphere-2026-360
Preprint. Discussion started: 13 February 2026

temperature, and water vapor mixing ratio. The 00 CST was selected since the inertial oscillation is the strongest at this time (Figure 10).

In May, the Great Plains LLJ in CTRL is embedded in strongly sloping isentropes, representing a typical springtime baroclinic environment (Fig. 11a). Under the PGW scenario, a distinct uneven warming pattern appears in the middle-to-upper levels, with stronger warming to the west and weaker warming to the east (Fig. 11c). This structure enhances the horizontal temperature gradient within the jet layer and strengthens the associated pressure gradient force. Consistent with this thermal adjustment, the meridional wind shows a coherent enhancement throughout the jet layer (Fig. 11b), indicating a strengthened background gradient wind that is toward the slope. And under the Coriolis force, the southerly geostrophic component gets enhanced. The moisture field adjusts coherently with the temperature structure. The increase in water vapor during May is not limited to the near-surface valley but also extends westward into the jet core region (Fig. 11d). Regions of stronger moistening generally coincide with weaker warming, reflecting a redistribution of energy between sensible and latent heat. This coupled warm–moist adjustment further enhances the thermal gradient near the Great Plains S-LLJ and modifies the virtual temperature and density fields, thereby providing additional thermodynamic support for the strengthened background geostrophic wind.

Figure 11e shows that the baroclinic structure is significantly weaker in August than in spring. Under the PGW scenario, potential temperature changes are mainly shown as the uniform background warming throughout the entire layer. Unlike in May, no significant strong warming band is observed from the central to western parts of the jet (Fig. 11g), so a stronger horizontal temperature gradient is not established within the jet layer. Therefore, the meridional wind changes display alternating positive and negative anomalies within the jet layer, lacking a growing structure (Fig. 11f). Besides, the increase in water vapor in August is confined to the eastern valley and upper levels, showing a weakened coupling with the core jet (Fig. 11h). Since the high moisture growth does not reach the jet, their modulation of the baroclinic structure is significantly weaker than in spring. Thus, climate change cannot effectively amplify the thermal gradient within the jet layer. This means that the background pressure gradient and the associated geostrophic wind do not undergo systematic strengthening. The magnitude of geostrophic wind changes in August is notably weaker than in May as a result.

https://doi.org/10.5194/egusphere-2026-360
Preprint. Discussion started: 13 February 2026

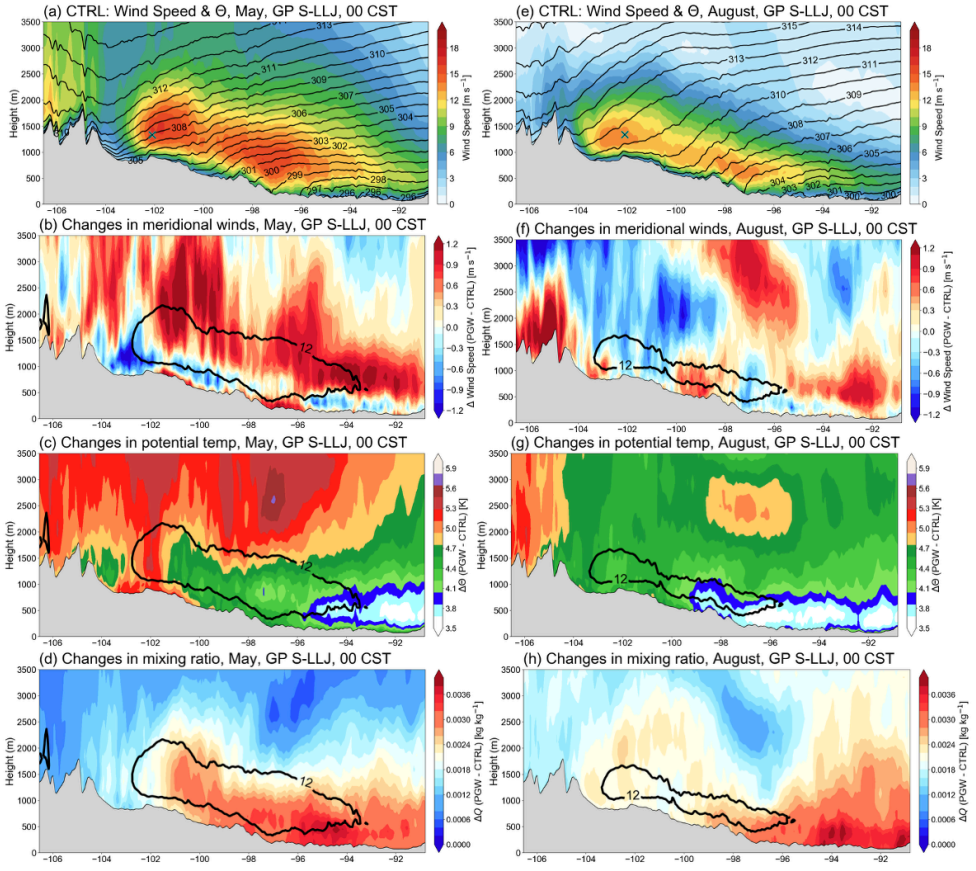

Figure 11. Meridional cross-section through Point A for (a–d) May and (e–h) August at 00 CST: (a, e) Mean wind speed (shading) and potential temperature (black contours) in the CTRL scenario; (b, f) changes in meridional wind; (c, g) changes in potential temperature; and (d, h) changes in water vapor mixing ratio. The black contours indicate the low-level jet core region (12 m/s).

Figure 12 further supports the seasonal differences in inertial oscillation response from the perspective of stability structure. The Richardson number (Ri) was used here to characterize boundary-layer stability quantitatively (Ri > 1 for stable conditions and Ri < 0.25 for turbulent conditions). Comparing figures 12a and b, the spring nocturnal near-surface unstable structure significantly weakens and even disappears from the valley to the highlands in the PGW simulation. Below the jet layer (−104 to −98), the Ri shows overall positive anomalies, implying that turbulent mixing is more easily suppressed at night (fig. 12c). The decoupling between the upper air of the boundary layer and surface is therefore enhanced in the future spring. This benefits the development of stronger inertial oscillations and amplifies the diurnal variation amplitude of LLJs.

However, the midnight unstable structure in August is enhanced in the PGW simulation. The Ri below the jet is dominated by negative anomalies (fig. 12f), which reveal more active turbulent mixing, and the air flow in the jet layer gets more influence from surface friction. As a result, under the mid-summer background, the conditions for

https://doi.org/10.5194/egusphere-2026-360
Preprint. Discussion started: 13 February 2026

inertial oscillation are not reinforced but instead tend to weaken. This behaviour is consistent with the August LLJ features shown in Fig. 10.

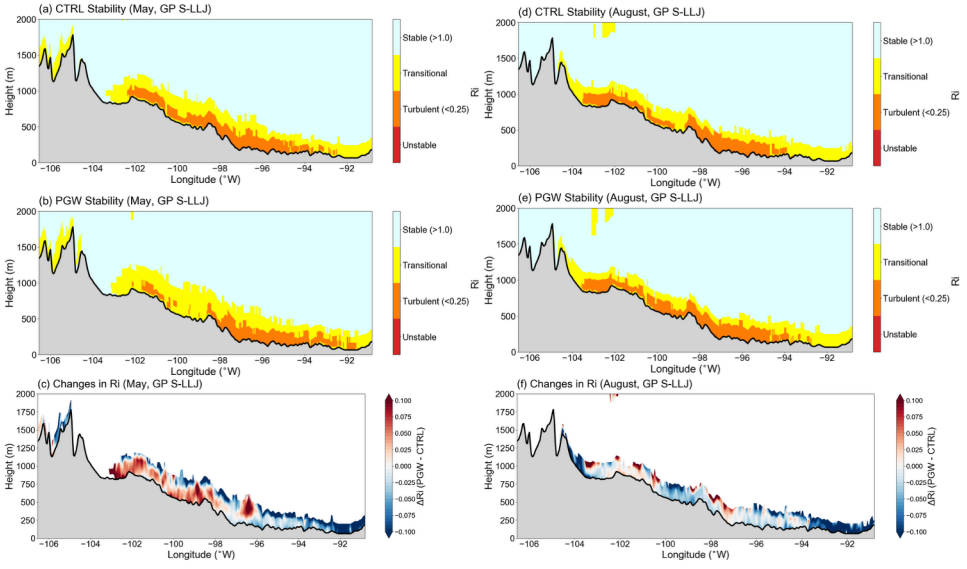

Figure 12. Cross-sections of stability structure and its changes associated with the Great Plains S-LLJ. (a, b) Stability classification based on the Richardson number (Ri) in May under the CTRL and PGW scenarios, respectively. (c) Changes in Ri (PGW − CTRL) in May. (d, e) As in (a, b), but for August. (f) Changes in Ri (PGW − CTRL) in August.

4.2 California coastal N-LLJ

Based on Section 3.3, May and July are selected to represent spring and summer for the California coastal N-LLJ. Point B is chosen for analysis because it is near the coast, where more frequent LLJs occur, and shows clearly contrasting responses to climate change between the two seasons. As noted in Ma et al. (2024), this jet is primarily controlled by the background geostrophic wind rather than inertial oscillation.

Figure 13 displays the mean geostrophic wind vectors and diurnal hodographs at the jet core height. In both May and July, the geostrophic winds are strong, while the actual wind hodographs show a weak diurnal cycle without a standard circular shape. Notably, the mean geostrophic wind becomes stronger in the PGW simulation in May, but slightly weaker in July. Since this LLJ is geostrophically driven, these changes in background flow directly explain the different seasonal responses at Point B. Moreover, at almost all time steps, the ageostrophic deviation is oriented opposite to the geostrophic wind. This indicates that a supergeostrophic state does not develop and that the actual wind remains subgeostrophic throughout the diurnal cycle. Therefore, the California coastal N-LLJ is mainly maintained by the background geostrophic flow and is continuously damped by surface friction, rather than being enhanced by nocturnal inertial oscillation

https://doi.org/10.5194/egusphere-2026-360
Preprint. Discussion started: 13 February 2026

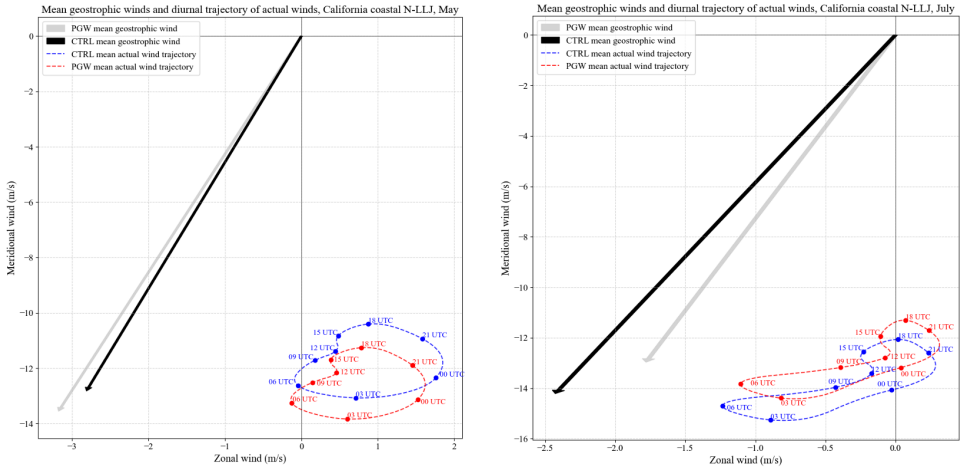

Figure 13. Mean geostrophic winds and the diurnal variation of actual winds at the core height of the N-LLJ over the California coast: (a) May, (b) July.

Thus, the mechanisms underlying the seasonal changes in the California coastal N-LLJ can be further interpreted from the perspective of background thermodynamic circulation. The time of 19:00 PST (03:00 UTC) is selected as a representative stage, because the coastal N-LLJ typically reaches its maximum intensity at this time (Fig. 13).

Under the present climate (Figs. 14a and 14d), the intensity and vertical structure of the California coastal N-LLJ are generally similar in spring and summer. In both seasons, the jet is embedded in a typical coastal baroclinic environment associated with the cool ocean and warm land contrast. However, the PGW-induced changes in the meridional wind show clear seasonal differences (Figs. 14b and 14e). The coastal jet layer is mainly featured by enhanced northerly flow in May, reflected by negative meridional wind anomalies, indicating a strengthening of the coastal N-LLJ. Whereas the positive meridional wind anomalies dominate in summer, from the middle troposphere down to the near-coastal boundary layer (approximately −126° to −125°), implying a widespread weakening of the northerly jet. But for the west of 126° W, weak northerly increase is still maintained near 400–500 m, but it is much more limited in both magnitude and spatial extent.

The changes in the temperature field further explain the seasonal contrast in the California coastal N-LLJ response. The potential temperature changes are closely aligned with the slope of the isentropes in May, extending from approximately 500 m to 2000 m (Fig. 14c). This structure is consistent with the typical feature of future warming, in which ocean warming is weaker than land warming. As a result, the land–sea thermal contrast and the associated baroclinicity near the jet layer are enhanced, which exerts a positive effect on strengthening the background geostrophic wind and the coastal N-LLJ.

The situation in July is notably different (Fig. 14f). Although the $\Delta\theta$ isolines in the lower boundary layer remain tilted, the main descending branch shifts westward from the coastal zone to offshore regions west of 125° W. This indicates that the strongest land–sea thermal contrast is displaced offshore. Consistent with this feature, a pronounced surface warming signal appears near 125° W in July. More importantly, a relative minimum centre

https://doi.org/10.5194/egusphere-2026-360
Preprint. Discussion started: 13 February 2026

of potential temperature warming is evident at about 300–500 m above −125° W, which directly weakens the baroclinic structure at the jet-core height. This thermal configuration disrupts the coastal baroclinicity and exerts a negative effect on the strength of the California coastal N-LLJ.

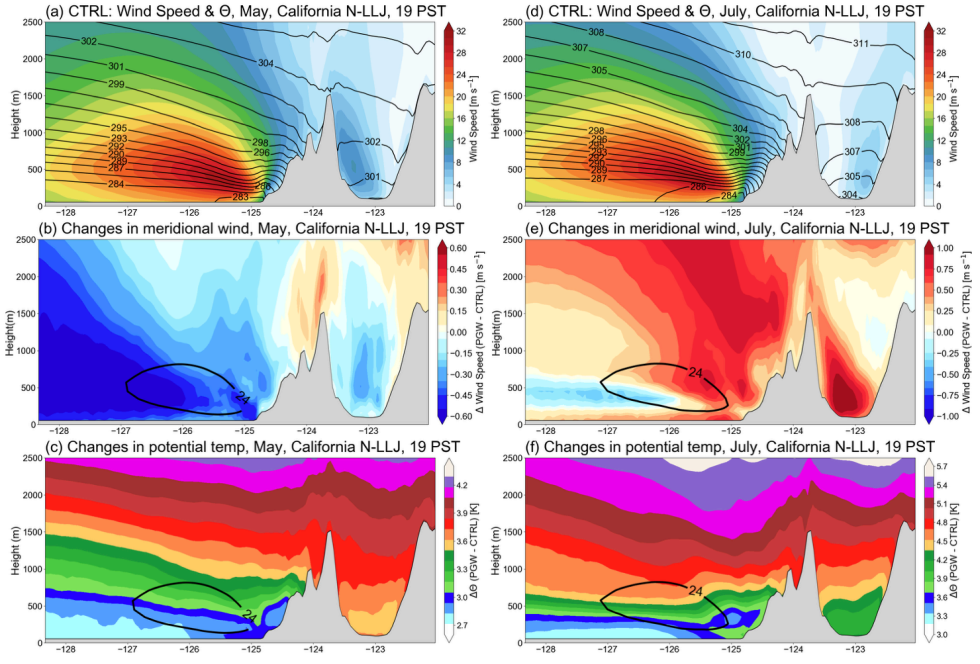

Figure 14. Meridional cross-section through Point B for (a–c) May and (d–f) July at 19 PST: (a, d) Mean wind speed (shading) and potential temperature (black contours) in the CTRL scenario; (b, e) changes in meridional wind; (c, f) changes in potential temperature. The black contours indicate the strong low-level jet core region (24 m/s).

The changes in the zonal wind further help interpret the near-coastal thermal adjustment (Fig. 15). Under the present-day climate, the coastal thermal configuration of this area (Fig. 14b) can be featured by a cold ocean - warm coastline - hot mountain, which supports a coupled sea-breeze and upslope-flow system. Under future warming, surface temperature increases near the coastline and offshore region are more pronounced in summer (Fig. 14f). Thermodynamically, this configuration tends to strengthen the onshore sea breeze, while the upslope flow becomes relatively weaker. This contrast is clearly proved in the zonal wind response (Fig. 15b). As a result, a low-level convergence zone is likely to form near the coast around 125° W in summer. The stronger sea breeze benefits cooler updraft in this region, which provides a dynamical explanation for the relative minimum centre in potential temperature warming above the coast. Although a slightly stronger offshore warming signal can also be identified in spring, it is much weaker than in summer. Consequently, the zonal wind changes in May do not exhibit a similarly strong contrast (Fig. 15a).

https://doi.org/10.5194/egusphere-2026-360
Preprint. Discussion started: 13 February 2026

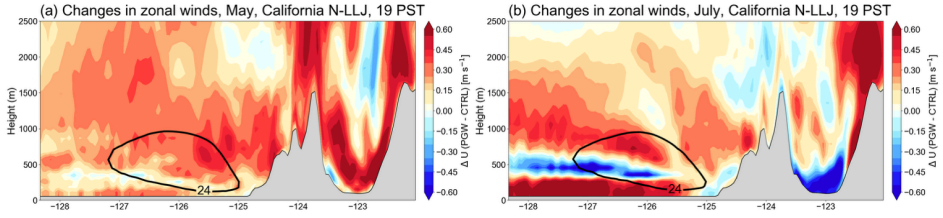

Figure 15. Meridional cross-section through Point B for the changes in zonal wind components. (a) May; (b) July at 19 PST.

5. Conclusion

This study used a convection-permitting WRF model to investigate how LLJs respond to climate change over North America. Previous projections of LLJ changes have primarily relied on global or coarse-resolution regional climate models, which have been widely used to analyze the large-scale circulation adjustments associated with future LLJ changes (Zhou et al., 2021). While these studies have established that LLJs are likely to change under climate warming, their coarse resolution limits the representation of jet-core structure and boundary-layer processes, particularly over complex terrain and coastal environments. In contrast, the convection-permitting simulations used here explicitly resolve jet heights, thermodynamic stratification, providing a physical basis for interpreting future LLJ responses.

The results reveal that the response of North American LLJs to climate warming is highly heterogeneous across seasons and regions, rather than a uniform intensification. The most pronounced strengthening of the Great Plains S-LLJ occurs in spring, with occurrence frequency increasing by approximately 3% and core wind speeds rising by more than 0.5 m s^{-1}. However, the summer response is strongly muted, characterized by limited intensity changes and a reduced amplitude of the diurnal cycle. This change differs from the study by Tang et al. (2017), which emphasized that enhancement predominantly occurs at night during summer and varies in frequency. The discrepancy arises because convection-permitting simulations explicitly resolve the warming-induced increase in nocturnal boundary-layer instability, which suppresses decoupling and damps the inertial oscillation, thereby limiting summer LLJ strengthening.

This study also projects that the California coastal N-LLJ exhibits enhanced jet activity in spring and autumn, but a pronounced summer weakening accompanied by an offshore shift of the jet core. This behaviour contrasts with large-scale or coarse-resolution projections that primarily emphasize monotonic changes in coastal wind strength and indicates that future coastal LLJ responses are governed not simply by background circulation changes, but by a reorganization of coastal boundary-layer structure and sea-breeze–baroclinicity interactions that can only be captured at convection-permitting scales.

Following the conceptual framework of Ma et al. (2024), we attribute these differential responses to distinct alterations in thermodynamic forcing and boundary layer stability under the PGW simulation. As to the Great Plains S-LLJ, the spring intensification is driven by a coupled thermal-dynamic adjustment. A steepened east-west temperature gradient enhances the background geostrophic southerlies, while increased nocturnal stability

https://doi.org/10.5194/egusphere-2026-360
Preprint. Discussion started: 13 February 2026

suppresses turbulent mixing, thereby amplifying the inertial oscillation. Conversely, in summer, the warming pattern is spatially uniform, preventing the enhancement of the baroclinic zone. Furthermore, increased nocturnal instability in summer weakens the decoupling of the boundary layer, dampening the inertial oscillation mechanism.

Whereas, for the California coastal N-LLJ, the summer weakening is dynamically linked to the reconfiguration of the land-sea thermal contrast. Although the land warms faster than the ocean, the maximum warming centres shift, and enhanced sea-breeze circulation disrupts the coastal baroclinicity at the jet core height (~300–500 m). This highlights that future LLJ evolution is not solely determined by large-scale thermal gradients but is critically modulated by local coastal circulations, that are poorly represented in coarse-resolution projections.

These results provide a dynamic reference for understanding the future evolution of low-level wind systems in North America and also offer a more physically constrained explanatory framework for interdisciplinary fields such as regional hydroclimate, extreme weather environments, and offshore wind energy assessment. The strengthening of the Great Plains S-LLJ in spring suggests a potential increase in moisture transport toward the central US, which could push the initiation of mesoscale convective systems (MCSs) and heavier spring precipitation or even tornadoes. Additionally, the projected vertical and zonal shift of jet core areas over the California coast, this also poses new considerations for wind energy assessment. The vertical wind shear and resource availability at current offshore wind farms may deviate from historical norms.

Overall, this study demonstrates that climate change reshapes not only the frequency and intensity of LLJs but also their vertical structure and governing mechanisms, giving a dimension of LLJ response largely unresolved in previous coarse-resolution projections. By explicitly simulating boundary-layer stability and coastal circulation adjustments, convection-permitting simulations provide a physically grounded framework for interpreting future low-level wind system changes. Nevertheless, several limitations remain. The 13-year simulation period is insufficient to fully characterize long-term climate variability and low-frequency internal variability. However, for convection-permitting climate simulations covering the entire North American continent, this configuration represents a practical balance between computational cost and physical realism. Future research should further examine interactions between LLJs and extreme weather systems to deepen the understanding of low-level wind responses under climate change.

https://doi.org/10.5194/egusphere-2026-360
Preprint. Discussion started: 13 February 2026

Acknowledgments

All authors thank the support of the NSERC Discovery Grant and the NSERC Alliance the Northern Hail Project.

Data Availability Statement

The WRF simulation over CONUS I can be accessed at Research Data Archive of NCAR https://rda.ucar.edu/datasets/ds612.0/.

Author contribution

Xiao Ma: Conceptualization; data curation; formal analysis; investigation; methodology; visualization; writing-original draft.

Yanping Li: Conceptualization; funding acquisition; investigation; methodology; project administration; supervision; validation; writing-review and editing.

Fei Huo: Data curation; methodology; validation; visualization; writing-review and editing.

Zhenhua Li: Data curation; methodology; validation; writing-review and editing.

Competing interests

All authors disclosed no relevant relationships.

https://doi.org/10.5194/egusphere-2026-360
Preprint. Discussion started: 13 February 2026

References

Banta, R. M., Y. L. Pichugina, N. D. Kelley, B. Jonkman, and W. A. Brewer (2008), Doppler lidar measurements of the Great Plains low-level jet: Applications to wind energy, IOP Conference Series: Earth and Environmental Science, 1, 012020, doi:10.1088/1755-1315/1/1/012020.

Blackadar, A. K. (1957), Boundary layer wind maxima and their significance for the growth of nocturnal inversions, Bulletin of the American Meteorological Society, 38(5), 283–290, doi:10.1175/1520-0477-38.5.283.

Bonner, W. D.: CLIMATOLOGY OF THE LOW LEVEL JET, Monthly Weather Review, 96(12), 833–850, doi:10.1175/1520-0493(1968)096<0833:cotllj>2.0.co;2, 1968.

Doubler, D. L., J. A. Winkler, X. Bian, C. K. Walters, and S. Zhong (2015), An NARR-derived climatology of southerly and northerly low-level jets over North America and Coastal Environs, Journal of Applied Meteorology and Climatology, 54(7), 1596–1619, doi:10.1175/jamc-d-14-0311.1.

Gadde, S. N., and R. J. Stevens (2021), Effect of low-level jet height on wind farm performance, Journal of Renewable and Sustainable Energy, 13(1), doi:10.1063/5.0026232.

Hodges, D., and Z. Pu (2019), Characteristics and variations of low-level jets and environmental factors associated with summer precipitation extremes over the Great Plains, Journal of Climate, 32(16), 5123–5144, doi:10.1175/jcli-d-18-0553.1.

HOLTON, J. R. (1967), The diurnal boundary layer wind oscillation above sloping terrain, Tellus, 19(2), 199–205, doi:10.1111/j.2153-3490.1967.tb01473.x.

Hong, S.-Y., Y. Noh, and J. Dudhia (2006), A new vertical diffusion package with an explicit treatment of entrainment processes, Monthly Weather Review, 134(9), 2318–2341, doi:10.1175/mwr3199.1.

Hu, X.-M., P. M. Klein, M. Xue, J. K. Lundquist, F. Zhang, and Y. Qi (2013), Impact of low-level jets on the nocturnal urban heat island intensity in Oklahoma City, Journal of Applied Meteorology and Climatology, 52(8), 1779–1802, doi:10.1175/jamc-d-12-0256.1.

Iacono, M. J., J. S. Delamere, E. J. Mlawer, M. W. Shephard, S. A. Clough, and W. D. Collins (2008), Radiative forcing by long-lived greenhouse gases: Calculations with the AER radiative transfer models, Journal of Geophysical Research: Atmospheres, 113(D13), doi:10.1029/2008jd009944.

Li, Y., Z. Li, Z. Zhang, L. Chen, S. Kurkute, L. Scaff, and X. Pan (2019), High-resolution regional climate modeling and projection over Western Canada using a weather research forecasting model with a pseudo-global warming approach, Hydrology and Earth System Sciences, 23(11), 4635–4659, doi:10.5194/hess-23-4635-2019.

Liu, C. et al. (2017), Continental-scale convection-permitting modeling of the current and future climate of North America, Climate Dynamics, 49(1–2), 71–95, doi:10.1007/s00382-016-3327-9.

Ma, X., Y. Li, and Z. Li (2022), The projection of Canadian wind energy potential in future scenarios using a convection-permitting regional climate model, Energy Reports, 8, 7176–7187, doi:10.1016/j.egyr.2022.05.122.

Ma, X., Y. Li, Z. Li, and F. Huo (2024), Investigation of the characteristics of low-level jets over North America in a convection-permitting weather research and forecasting simulation, Atmospheric Chemistry and Physics, 24(20), 12013–12030, doi:10.5194/acp-24-12013-2024.

Mu, Y., C. Jones, L. M. Carvalho, J. Kukulies, A. F. Prein, L. Xue, and C. Liu (2025), Impacts of northerly low-level jets on mesoscale convective systems east of the Andes, Journal of Geophysical Research: Atmospheres, 130(21), doi:10.1029/2025jd043842.

https://doi.org/10.5194/egusphere-2026-360
Preprint. Discussion started: 13 February 2026

Niu, G.-Y. et al. (2011), The community Noah Land Surface Model with multiparameterization options (Noah-MP): 1. model description and evaluation with local-scale measurements, Journal of Geophysical Research, 116(D12), doi:10.1029/2010jd015139.

Rife, D. L., J. O. Pinto, A. J. Monaghan, C. A. Davis, and J. R. Hannan (2010), Global distribution and characteristics of diurnally varying low-level jets, Journal of Climate, 23(19), 5041–5064, doi:10.1175/2010jcli3514.1.

Semedo, A., P. M. M. Soares, D. C. A. Lima, R. M. Cardoso, M. Bernardino, and P. M. A. Miranda (2016), The impact of climate change on the global coastal low-level wind jets: EC-Earth Simulations, Global and Planetary Change, 137, 88–106, doi:10.1016/j.gloplacha.2015.12.012.

Stensrud, D. J. (1996), Importance of low-level jets to climate: A Review, Journal of Climate, 9(8), 1698–1711, doi:10.1175/1520-0442(1996)009<1698:iolljt>2.0.co;2.

Tang, Y., J. Winkler, S. Zhong, X. Bian, D. Doubler, L. Yu, and C. Walters (2017a), Future changes in the climatology of the Great Plains low-level jet derived from fine resolution multi-model simulations, Scientific Reports, 7(1), doi:10.1038/s41598-017-05135-0.

Tang, Y., J. Winkler, S. Zhong, X. Bian, D. Doubler, L. Yu, and C. Walters (2017b), Future changes in the climatology of the Great Plains low-level jet derived from fine resolution multi-model simulations, Scientific Reports, 7(1), doi:10.1038/s41598-017-05135-0.

Taylor, K. E., R. J. Stouffer, and G. A. Meehl (2012), An overview of CMIP5 and the experiment design, Bulletin of the American Meteorological Society, 93(4), 485–498, doi:10.1175/bams-d-11-00094.1.

Torres-Alavez, J. A., S. Das, A. Corrales-Suastegui, E. Coppola, F. Giorgi, F. Raffaele, M. S. Bukovsky, M. Ashfaq, J. A. Salinas, and T. Sines (2021), Future projections in the climatology of global low-level jets from CORDEX-core simulations, Climate Dynamics, 57(5–6), 1551–1569, doi:10.1007/s00382-021-05671-6.

Uccellini, L. W., R. A. Petersen, P. J. Kocin, K. F. Brill, and J. J. Tuccillo (1987), Synergistic interactions between an upper-level jet streak and diabatic processes that influence the development of a low-level jet and a secondary coastal cyclone, Monthly Weather Review, 115(10), 2227–2261, doi:10.1175/1520-0493(1987)115<2227:sibaul>2.0.co;2.

Walters, C. K., J. A. Winkler, R. P. Shadbolt, J. van Ravensway, and G. D. Bierly (2008), A long-term climatology of southerly and northerly low-level jets for the Central United States, Annals of the Association of American Geographers, 98(3), 521–552, doi:10.1080/00045600802046387.

Weaver, S. J., S. Baxter, and A. Kumar (2012), Climatic role of North American low-level jets on U.S. Regional Tornado activity, Journal of Climate, 25(19), 6666–6683, doi:10.1175/jcli-d-11-00568.1.

Zhang, Z., Chen, F., Barlage, M., Bortolotti, L. E., Famiglietti, J., Li, Z., Ma, X. and Li, Y.: Cooling effects revealed by modeling of wetlands and land-atmosphere interactions, Water Resources Research, 58(3), doi:10.1029/2021wr030573, 2022.

Zhou, W., L. R. Leung, F. Song, and J. Lu (2021), Future changes in the Great Plains Low-level jet governed by seasonally dependent pattern changes in the North Atlantic Subtropical high, Geophysical Research Letters, 48(4), doi:10.1029/2020gl090356.